HHS Public Access

Author manuscript

NanoImpact. Author manuscript; available in PMC 2019 April 01.

Published in final edited form as:

NanoImpact. 2018 April ; 10: 26–37. doi:10.1016/j.impact.2017.11.007.

Development of reference metal and metal oxide engineered nanomaterials for nanotoxicology research using high throughput and precision flame spray synthesis approaches

Juan Beltran-Huarac[a], **Zhenyuan Zhang**[a], **Georgios Pyrgiotakis**[a], **Glen DeLoid**[a], **Nachiket Vaze**[a], **Saber M. Hussain**[b], and **Philip Demokritou**[a,*]

[a]Center for Nanotechnology and Nanotoxicology, HSPH-NIEHS Nanosafety Center, Department of Environmental Health, Harvard T. H. Chan School of Public School, Harvard University, Boston, MA 02115, USA

[b]Molecular Bioeffects Branch, Airman Systems Directorate, Wright Patterson Air Force Base, Dayton, OH, USA

Abstract

There is a growing need to develop and characterize reference metal and metal oxide engineered nanomaterials (ENMs) of high purity and tunable intrinsic properties suitable for nanotoxicology research. Here a high throughput (volume) and precision flame spray pyrolysis (FSP) approach coupled with state-of-the-art characterization techniques are utilized to generate such reference ENMs. The lab-based and industrially relevant FSP system, termed as Versatile Engineered Nanomaterials Generation System (VENGES), synthesizes the metals and metal oxides, at high throughput manner with controlled properties, such as primary particle size, aggregate diameter, shape, crystallinity, stoichiometry and surface chemistry. A nanopanel of nine reference ENMs (silica, silver, silver supported on silica, alumina, ceria and iron oxide) was synthesized and characterized using combined electron microscopy, advanced spectroscopic techniques and physical analyses (*e.g.*, BET, XRD, TEM, pycnometry, XPS, ICP-MS and FTIR). ENMs show a high degree of chemical purity and stoichiometry, and low content of carbon residuals, and are sterile and free of bacteria and endotoxins. Further, their colloidal properties and their implication in *in-vitro* dosimetry have been also investigated in both environmental and test biological media. The suitability of reference ENMs and protocols developed in this study brings forth new arenas to generate reliable and reproducible toxicological data in an effort to reduce conflicting and contradicting inter-laboratory data on relative toxic effects of ENMs.

Keywords

Reference Materials; Nanotoxicology; Engineered nanomaterials; Nano-bio interactions; Dosimetry; Metal Oxides

*Corresponding author. pdemokri@hsph.harvard.edu.

1. Introduction

Since engineered nanomaterials (ENMs) are currently being utilized extensively in industry, incorporated into consumer products, and employed in medical imaging and therapeutic applications (McClements et al., 2016; Eleftheriadou et al., 2017; Servin et al., 2016; Pal et al., 2015a, 2015b; Pirela et al., 2016a; Keller et al., 2013; Roco et al. 2011), the comprehensive understanding of the relationship between the physicochemical properties of ENMs and their biological activity is of paramount importance. Despite the progress made the last 10 years there are still major gaps in understanding ENM toxicity, conflicting and contradictory data on toxicity and potential environmental health, and safety risks from such inevitable exposures (Chalbot et al., 2017; Pirela et al., 2016a, 2016b; McClements et al., 2016; Pal et al., 2015a) across the life cycle of nano-enabled products.

Among the leading reasons for such conflicting toxicological data on ENMs is the lack of an extensive library of industrially relevant ENMs, inadequate characterization of ENMs both at the “pristine” phase and in relevant biological and environmental media, lack of harmonized methodologies for dispersion preparation and colloidal characterization, and finally the absent of dosimetry considerations that takes the ENM interactions in liquid into account (Pal et al., 2015a, 2015b; Cohen et al., 2015). Another issue is the lack of standardized ENMs that have the potential to homogenize inconsistencies of toxicological data. Standardized ENMs are usually categorized into test ENMs, reference ENMs and certified reference ENMs. A test ENM is often used in basic research for the development of protocols or instrumentation (Stone et al., 2010). Following the ISO definitions (ISO/Guide 30:2015), a reference ENM is a “material, sufficiently homogeneous and stable with respect to one or more specified properties, which has been established to be fit for its intended use in a measurement process”, whereas a certified reference ENM is a “reference material characterized by a metrologically valid procedure for one or more specified properties, accompanied by an reference material certificate that provides the value of the specified property, its associated uncertainty, and a statement of metrological traceability”. Despite the ease of this terminology, the development of such standardized ENMs in practice represents a hurdle to overcome. To date, there are some initiatives underway to develop standardized ENMs. For instance, it is worth of remark the efforts made by OECD and NIST to make available test ENMs and certified reference ENMs, respectively, for nanotechnology research. The NIST certified reference ENMs are however mainly limited to silver, gold, titanium dioxide and silicon ENMs of a few sizes and chemistries, whereas OECD test ENMs are representative and commercially available ENMs, procured and characterized and may suffer from the known batch-to-batch and source-to-source variability, impurities and their structure/property is limited to whatever is commercially available, among other issues. In this context, the availability of reference ENMs with controlled properties suitable for nanotoxicology research remains a big challenge.

Reference ENMs suitable for nanotoxicology research need to have unique features. For instance, in order to elucidate the ENM structure/activity relationships and relate the physicochemical and morphological properties of ENMs to their biological activity (Cohen et al., 2017; Taurozzi et al. 2011; Pradhan et al., 2016), there is a need to synthesize reference ENMs that exhibit precisely controlled properties in a reproducible manner.

Moreover, reference ENMs must be generated at the high volumes needed for *in-vivo* and *in-vitro* toxicological studies, be free of biological origin contaminants (bacteria, endotoxins, etc.) and of high purity and quality (no organics, carbon residues, etc), and with stable and homogeneous properties over time. Furthermore, their intrinsic properties (including primary size, size distribution, surface charge, crystal structure, agglomeration state, surface area, porosity, morphology, chemical composition and purity) must be well characterized by state-of-the-art methodologies. Such property values also need to be accompanied by an uncertainty at an established level of confidence (ISO Guide 1992, 2007). In addition, reference ENMs in powder form and suspensions need to be rigorously and extensively characterized.

Among the physical, chemical and morphological characterization techniques used to characterize reference ENMs are Brunauer-Emmett-Teller (BET), X-ray diffraction (XRD), transmission electron microscopy (TEM), pycnometry, X-ray photoelectron spectroscopy (XPS), inductively coupled plasma - mass spectrometry (ICP-MS), Fourier transform infrared (FTIR), dynamic light scattering (DLS) and elemental carbon – organic carbon (EC-OC) thermal optical analysis (Nanda et al., 2012; Barret et al., 1951; Burnett et al., 2010; Bish et al., 1988; Monecke et al., 2001; Wang et al., 2000; Pyrz et al., 2008; Beauchemin et al., 2010; Grant et al., 1989). In addition to the traditional characterization of intrinsic properties of reference ENMs, it is critically important that the extrinsic properties (such as agglomeration size and state, dissolution, pH, zeta potential and effective density) of reference ENMs in environmental and biological media be also characterized. The importance of characterization of ENM transformations in biological and environmental media, and the effect in bioactivity and particle-kinetics in *in-vitro* cellular systems is well documented in the literature (McClements et al., 2016; Pal et al., 2015a, 2015b; DeLoid et at., 2015, 2016, 2017; Cohen et al., 2013, 2014a, 2014b; Molina et al., 2014; Watson et al., 2014; Pyrgiotakis et al., 2013, 2014a; Demokriotu et al., 2013; Bello 2013; Sotiriou 2012; Vilanova et al., 2016) and must be taken into consideration. The suspension preparation, colloidal characterization, and in-vitro dosimetry analysis of dispersed ENMs in biological media is a pivotal key for cellular toxicology research (Cohen et al., 2014). It is well known that ENMs in suspension are subject to ENM- and media-specific physicochemical transformations that affect not only their bioactivity due to protein corona formation (Pyrgiotakis et al., 2013, 2014b; Tsuda et al., 2016) but also their fate and transport in vitro, and in turn the dose delivered to cells as a function of exposure time (DeLoid et al., 2017). Recent studies have showcased the potential effects of dosimetry on hazard ranking of large panels of low-aspect ratio ENMs (Pal et al 2015a, 2015b). Notwithstanding, while for isotropic ENMs with low aspect ratios, standardized methodologies across the ENM dispersion preparation-colloidal characterization-dosimetry have been developed and validated (DeLoid et al., 2017), the subject represents a big challenge for emerging anisotropic materials.

Another important element, often overlooked, related to reference ENMs is their short- and long-term storage and potential property transformations at various environmental conditions, which may introduce bias in biological studies and is one of the reasons for the inconsistences in the nanotoxicology literature (Petersen et al., 2014). It has been reported that under various environmental conditions, such as daylight, relative humidity and

temperature, certain ENMs can be physicochemically “aged” over time, which can have an effect on their biological properties (Petersen et al., 2014; Glover et al., 2011; Izak-Nau et al., 2015; El Badawy et al., 2010). Such temporal property changes in the case of metal/metal oxides may give rise to the release of metallic ions and induce toxicity upon altering their agglomeration state, dissolution rate and surface charge (Izak-Nau et al., 2015). Therefore, it is imperative that the reference ENMs are stored in environmentally controlled and inert conditions (*i.e.* absence of oxygen, moisture and UV light, and under controlled temperature). Their key properties must be also monitored over time to assess potential modifications and to keep the physicochemical integrity of ENMs unaltered. In terms of the potential contamination in pre- and post-synthesis, the reference ENMs must be screened for contaminants of bacterial and endotoxin origin that are adsorbed onto the reactive surface of ENMs. ENMs can get contaminated with endotoxin during synthesis, handling, transfer or storage (Oostingh et al., 2011). It is worth noting that the surface area of ENMs is much higher than that of its bulk counterparts, *i.e.*, a much higher proportion of atoms are at the surface and consequently greater propensity for reaction. Thus, the cumulative presence of endotoxins on ENMs surface can mask realistic nano-bio interactions (inducing cell activation) and generate misleading *in-vitro* and *in-vivo* toxicological effects (Li et al., 2016). It has been reported that endotoxin contamination was found present in many commercially available ENMs used in nanotoxicology research (Sandle et al., 2013). It is worthy of remark that although there are some methods (including two-phase extraction, ultrafiltration, inactivation, gel filtration and ion-exchange chromatography, and plasma discharge) that can be used to remove endotoxins from ENMs, there is no gold standard for endotoxin removal (Li et al., 2016). More importantly, such methods can cause certain alterations in the physicochemical properties and stability of ENMs, which can introduce bias in toxicology assessment. Nonetheless, it is more efficient to incorporate aseptic techniques and screening of both raw materials used in synthesis and storage processes in place to minimize potential endotoxin contamination.

Here we report the synthesis and detailed characterization of reference metal and metal oxide ENMs of high purity and quality, and of tunable intrinsic properties suitable for nanotoxicology research. Such ENMs were developed as part of the Harvard-National Institute for Environmental Health Sciences (NIEHS) Reference ENM Repository developed at Harvard T. H. Chan School of Public Health. These reference ENMs will be utilized for nanotoxicology research as part of the Nanotechnology Health Implications Research (NHIR) Consortium established by NIEHS in 2016, and also available to other interested parties around the globe. A high throughput (volume) and precision FSP synthesis approach coupled with state-of-the-art characterization techniques are utilized to generate the reference metal and metal oxide ENMs. Special emphasis was given not only on the detailed physicochemical characterization of pristine ENMs but also on their colloidal characterization in environmental and biological test media, following a detailed protocol recently developed by the authors across the dispersion preparation-colloidal characterization-cellular dosimetry. The generated reference ENMs were rigorously characterized using advanced analytical techniques and thoroughly stored under argon-controlled environment to avoid property transformations. In addition, the sterility in terms

of bacterial and endotoxin contamination was assessed to ensure that there is no interference with biological assessment.

2. Materials and methods

2.1. High throughput, precision flame spray synthesis platform for reference ENMs generation using a versatile engineered nanomaterial generation system (VENGES)

ENMs were synthesized using the Harvard Versatile Engineered Nanomaterial Generation System (VENGES) via flame spray pyrolysis (FSP) method (Demokritou et al., 2010; Orts-Gil et al., 2013; Tsai et al., 2012; Glover et al., 2011). Flame aerosol technology represents more than 90% of the worldwide volume and value of nanostructured particle commodities produced in gas-phase (Wegner et al., 2003). The FSP system offers a high throughput synthesis of any functional metal/metal oxide and its related hierarchically-organized composites at large scale, and a precise control of its properties (including composition, size, phase and shape). It also enables high volume rates (~ few grams per hour) and an excellent reproducibility (Strobel et al., 2007). In contrast to other synthesis approaches (such as sol-gel and hydrothermal methods), FSP under high oxidation conditions produces ENMs free of organic residues on their outer surface (McPherson et al., 1980; Levin et al., 1998; Teleki et al., 2008; Teoh et al., 2010; Demokritou et al., 2010; Tsai et al., 2012; Wegner et al., 2003; Strobel et al., 2007). Such residues could eventually interfere with their bioactivity or protein corona formation, and introduce bias in biological screening (Teleki et al., 2008). The lab based VENGES setup is depicted in Fig. 1a. In more detail:

Synthesis of ENMs—The FSP process is described elsewhere in great detail (Demokritou et al., 2010; Tsai et al., 2012; Glover et al., 2011). Briefly, a solution is fed through a capillary with flow rate × (typically in ml/min). The solution contains a highly flammable solvent that has dissolved a metal oxide precursor of known concentration. As the precursor solution is pumped out, an oxygen stream with flow y (typically in l/min) at the end of the capillary atomizes the precursor solution into fine droplets. A stoichiometric methane/oxygen flame ignites the precursor solution and the high heat that released converts the precursor to the metal oxide. A pump is used to collect the ENMs on a metal mesh (4000) supported on water-cooled glass fiber filter (Whatman®, 25.5 cm Ø). Occasionally, a quartz tube can be used to control the temperature profile across the reactor that can further enable the growth of the particles. In that case, a sheath flow of oxygen is used to supply the oxygen needed for the full combustion of the reagents, and to control the residence time in the tube. The various parameters such as the precursor concentration, the x/y ratio, sheath flow, and the solvent choice can be adjusted to control the ENM properties. Fine-tuning of these parameters can result in different shapes, sizes and configurations, as shown in Fig. 1b.

It is worth noting that the reproducibility of the method in terms of the properties of the synthesized ENMs is confirmed in this study. Multiple batches for each ENM were synthesized and key property characterization (such as BET, XRD and TEM) were compared to assess reproducibility. For each batch separately, we measured the specific surface area values allowing 10% variation and ±3nm variation in XRD/dBET values among

individual batches. This is in line with the literature (Teleki et al., 2008; Teoh et al., 2010; Wegner et al., 2003; Strobel et al., 2007).

Table S1 summarizes the experimental conditions used here to synthesize the reference ENMs. All chemicals were purchased from Sigma Aldrich and were ACS grade (99.9% purity). For all experiments, the pilot flame is kept identical at a flow rate of 3.2 and 1.5 L/min for CH_4 (Medtech, purity >99.9%) and O_2 (Airgas, purity >99.9%), respectively. The backpressure of the dispersion O_2 is usually regulated to 1.5–2.0 bar.

Storage and monitoring of reference ENMs—The ENMs collected on the filter were rapidly (<1 min) extracted and transferred into amber high-density polyethylene (HDPE) vials previously cleaned according to trace metals analysis protocols. The vials were stored in a glove box under argon environment (Unilab^{pro}SP, mBRAun) for further analysis. The environmental conditions inside the glovebox were maintained to O_2<0.1 ppm and H_2O<0.1 ppm. The glovebox also provides UV shielding.

2.2. Physicochemical and morphological characterization of reference ENMs

Primary particle size—Multiple methods were used to derive the primary particle size for the reference ENMs. In more detail:

TEM: Transmission electron microscopy (TEM, JEOL 2100) was also used to ascertain the primary particle size of ENMs. 2 mg of ENMs powders were first dispersed into 4 mL of deionized H_2O. The powder suspension was ultrasonicated for 4 min using a cup horn sonicator (Branson Digital Sonifier®) at 2.59 W/ml. One drop of this suspension was pipetted onto the TEM grids (Ted Pella Inc., Redding, CA), and was left to dry for 10 min. The remaining suspension was removed by absorption with a filter paper. Image analysis was performed using ImageJ software (supported by NIH). The average Feret diameter (FD) was used as the particle size and the standard deviation as the error of the particle size. The TEM instrument is calibrated periodically by the staff at the Department of Chemistry and Chemical Biology or service engineer at Harvard University. The CCD camera is calibrated once a month. Periodically images are obtained with a standard Gold nanoparticle suspension to ensure that the scale-bars are corresponding to the correct magnifications.

XRD: The primary particle size of ENMs was also determined via X-ray diffraction (XRD, Bruker D2 Phaser). The XRD patterns collected in 2θ 10–90° configuration (0.02° increment and 2s step) were analyzed by EVA software. The crystallite size was estimated based on the Scherrer's formula. The XRD instrument is calibrated periodically by the staff at the Department of Chemistry and Chemical Biology or service engineer at Harvard University.

BET: Brunauer-Emmett-Teller (BET) N_2-adsorption at 77K was conducted to determine the powder-specific surface area (SSA) of the ENMs. For this purpose, a high-throughput surface area and pore-size analyzer (Quantachrome Instruments, NOVAtouch LX^4) that follows a 5-point BET isotherm approach was used. Approximately 20–50 mg of ENMs in powder form was flushed with a N_2 gas at 100–300 °C for >3 h depending on the material. The BET primary particle size (dBET) was calculated under the assumption that the

particles are spherical and of equal size following dBET = 6000/(SSA·ρ), where the SSA is the specific surface are in m2/g, ρ is the material density in g/cm3, and dBET is in nm. The error calculation of the SSA value takes into consideration the SSA value and the error of the mass weighted for BET. The instrument is calibrated and checked for accuracy with Alumina standard once every 6 months or after 100 consecutive measurements.

Primary particle size distribution and shape factors—The size distribution and shape factors (aspect ratio, circularity and roundness) were determined by TEM (JEOL 2100) image analysis using ImageJ software. Note that all particles with discrete borders in each image were counted using the Feret diameter. A minimum of 100 particles was considered for the counting. Particles were counted until the distribution was not significantly (more than ±10%) changing with the addition of more particles. TEM images shown in this work are representative images of the particles.

Crystallinity—X-ray powder diffraction analysis using EVA software was used to ascertain the degree of crystallinity of ENMs. The calculation is obtained by dividing the total area under the crystalline peaks by the total area under the diffraction curve, which includes both the crystalline and amorphous peaks.

Porosity and density—The total pore volume (TPV) and average pore size (APS) were estimated using BET. TPV and APS are estimated employing the N2 adsorption isotherm approach (type H1 hysteresis), and derived from the amount of vapor adsorbed at a relative pressure P/Po at 0.995 and assuming a cylindrical-pore model. For ENMs, the pore volume should also be confirmed by TEM imaging since the inter-particle space could be counted as pore volume.

The density of ENMs in powder form was measured using a pycnometer (Quantachrome Instruments, ULTRAPYC 1200e) through N_2 volume displacement and the volume-to-pressure relationship known as Boyle's Law. ENM powder was used as is without any preparation. The ENM mass used ranges from 500 mg to 2 g based on the material density. The sample was analyzed a total of 15 times and the average value was used as the value of the density. The mass of ENM is weighted in 0.0001 g precision scale. The instrument is calibrated before each usage using standard spheres provided by Quantachrome Instruments. Gas flow rate and pressure is checked once a year to validate the instrument internal valves functionality.

Chemical composition, stoichiometry and surface chemistry—The elemental composition, trace metal purity, stoichiometry and chemical analysis of ENMs were analyzed via inductively coupled plasma – mass spectrometry (ICP-MS, Thermo-Finnigan Element 2). 1 mg of ENM powder is placed in a Teflon pressure vessel with a mixture made of 1.5 mL of 16 N HNO_3 and 0.2 mL of 12 N HCl. For the silica and silver/silica composites, 28 N HF was used. The samples are then heated up to 180 °C and vented/cooled for 1 h. After cooling, digests are diluted to 30 mL with high purity water prior to ICP-MS analysis. All vessels were pre-cleaned using an acid solution consisting of 2.4 N HCl for two days, then 3.2 N HNO_3 for two more days and then rinsed with high purity water. In addition to the collected samples, sample spikes, sample duplicates, blanks, standards and

certified reference materials (NIST 2709, NIST 1648a, NIST 2556, NIST 2702) were used in the chemical testing. The analysis included all 51 metals and Si. The XPS instrument is calibrated periodically by the staff at the CNS and the service engineer at Harvard University. The spectra are calibrated with respect to Si peak or C peak. A sample duplicate is run every 5 samples to ensure the precision of the instrument. The acceptable maximum peak of variability is 0.3 eV.

Molecular weight/stoichiometry calculation: Although ICP-MS does not measure directly oxygen content; it can be estimated by a mass-balance method assuming that the remaining mass is oxygen after correcting for elemental and organic carbon (see below).

The stoichiometry and surface chemical composition of ENMs were also ascertained via X-ray photoelectron spectroscopy (XPS, Thermo Scientific K-Alpha). A double side carbon tape was used to fix a pellet of the ENM powders on XPS platen. Approximately 50–100 mg of the ENM were placed on the carbon tape and pressed to form a pellet and adhere on the carbon tape. Five scans of survey were conducted to identify the elemental composition of material. The survey range was set from −10 eV to 1350 eV with 200 eV pass energy and 400 μm spot size. Three different spots of the pellet were used for the survey. Once all the elements have been identified high resolution elemental scans follow to all elements identified. The atomic ratio can be directly related to the stoichiometry of the ENM. However, for metal oxides it is likely that some of the oxygen can be due to various organic carbons on the surface of particles, which increases the relative oxygen ratio. To resolve this issue, if the carbon peak indicates more than 5% carbon, the elemental peaks for the oxygen is analyzed to separate the organic form of oxygen from the metal oxide form. The metal oxide peak is assigned to ~531 eV and the organic oxygen peak is assigned to the ~532 eV. Once the analysis is complete, the stoichiometry is calculated based on the metal oxide oxygen content and the result is given in the form of M_XO_Y. The XPS instrument is calibrated periodically by the staff at the CNS and the service engineer at Harvard University. The spectra are calibrated with respect to Si peak or C peak. A sample duplicate is run every 5 samples to ensure the precision of the instrument. The acceptable maximum peak of variability is 0.3 eV.

The surface functional groups of ENMs were determined and analyzed by Fourier transformed infrared (FTIR, Perkin Elmer) spectroscopy. FTIR spectra were collected in ATR mode. ENMs in powder form were directly placed on a cone shaped holder, and continuously scanned for 5 min. The XPS instrument is calibrated periodically by the staff at the CNS and the service engineer at Harvard University. Polystyrene Reference Standards are to use to calibrate the FTIR wavenumber accuracy (PIKE Technologies offers several versions of polystyrene reference materials for FTIR spectrometer calibration).

Carbon Content—Since FSP is a pyrolytic method that uses organic precursors, it is likely that there is elemental or organic carbon traces on the surface of ENMs (Teleki et al., 2008; Teoh et al., 2010; Wegner et al., 2003; Strobel et al., 2007). Thermal-optical analysis was used to measure the elemental carbon and organic carbon (EC/OC) content in the ENMs using a NIOSH 5040 method (Sunset Laboratory Inc.). A total of 1 mg of the ENMs were dispersed in 20 ml of DI water. The suspension was passed through a pre-baked Quartz fiber

filter via vacuum filtration, and the filters were then dried. The quartz filters (Pall Corporation, #7202) were baked at 300 °C to remove all absorbed carbon. The filters were then placed in a petri dish lined with aluminum, and sealed with Teflon tape until further usage. 10 ml of an ENM suspension at 150 μg/ml was passed through Quartz filter, using a glass vacuum filter holder (VWR, #89428-952). A control with just the water was also done to account for the organics present in the DI water. A major component of the measurement system of the EC/OC analyzer is the use of a fixed volume loop. This is used to inject an external standard of carbon at the end of every analysis. The external standard is used along with the known carbon concentration in the loop to calculate the analytical results.

2.3. Bacterial and endotoxin characterization of ENMs

The endotoxin levels present on ENMs were evaluated using the Recombinant Factor C (rFC) assay (EndoZyme®, Hyglos). ENMs were diluted to a starting concentration of between 0.5 and 10 μg/ml in endotoxin-free water (EndoZyme®, Hyglos) and the pH was adjusted to 7.0. The final concentration of ENMs was optimized separately for each ENM to minimize interference. Endotoxin-free water was used as a negative control and blank. The endotoxin standard stock provided with the kit was used to prepare samples at known concentrations for a standard curve (from 0.005 to 5.0 EU/ml). For each test sample, an identical sample spiked with 0.5 EU/ml of endotoxin was prepared to test for assay interference. Samples, spiked samples and standard dilutions were dispensed into a pre-warmed (37 °C) 96 well plate (100 μl/well), and mixed with 100 μl assay reagent (8:1:1 ratio of assay buffer, enzyme, and substrate). Fluorescence (Ex. 380, Em. 440) was measured at t=0 and at 90 minutes. Endotoxin levels were calculated from sample fluorescence using a standard curve equation generated from standard endotoxin dilutions. The presence of bacteria on ENMs was assessed following the USP pharmacopeia protocol (WHO document, QAS/11.413). Briefly, 1ml of each ENM suspension (0.5 mg/ml in deionized water) was added to 10ml of Fluid Thioglycollate Media (FTM) (Criterion, Hardy Diagnostics, Santa Maria CA). Each solution was then incubated at 37 °C inside a stationary incubator for 14 days. The solutions were monitored daily for any visible change in turbidity, which was further analyzed by spreading an inoculum of the solution to be examined onto a Tryptic Soy Agar (BD Biosciences San Jose CA), and incubating overnight inside a stationary incubator at 37 °C.

2.4. Suspension preparation, colloidal characterization and cellular dosimetric analysis of ENMs

The integrated methodology across the ENM dispersion preparation-characterization-cellular dosimetry presented here is based on a standardized protocol recently developed by our research group and published in Nature Protocols (DeLoid et al., 2017). Here we only summarize some quality aspects of this three-step methodology for the ENMs of interest as follows:

ENM suspension preparation and colloidal characterization—The cup horn sonicator (Branson Digital Sonifier®) was calibrated and found to deliver 2.59 W/ml. A stock solution of ENMs in DI water was prepared at a concentration of 0.5 mg/ml and was used to determine the critical delivered sonication energy (DSEcr). 1 ml of the stock solution

was used to measure the hydrodynamical diameter (dH) with DLS (Malvern Nanosizer, Worcestershire, UK). The solution was sonicated for 1 minute and measured again. The process continued until the dH and polydispersity index (PDI) were not changing significantly (±5%). The DSEcr of an ENM is defined as the DSE (in J/ml) required to achieve a monodisperse solution at the lowest particle agglomeration state in DI H_2O and is ENM-specific. All suspensions from that point on were prepared according to the DSEcr and were then adjusted to the desired concentration. It should be noted that the effect of sonication on dissolution of ENMs could also affect the levels of ions released from the particles being dispersed in water. But this point is out of focus of the present study.

Determination of suspended nanomaterial effective density in test biological media—Effective density (ρ_{eff}) was determined using the volumetric centrifugation method (VCM) as described previously (DeLoid et al., 2017). Briefly, 1.0 ml of 0.1 mg/ml ENM solution in RPMI+10%(vol/vol) FBS was dispensed in each of three packed cell volume (PCV) tubes, and centrifuged at room temperature for 1–6 hour at 3000–12000 × g depending on the ENMs. After centrifugation, the volume of the formed pellet was measured. The ρ_{eff} for each measured pellet was calculated as follows:

$$\rho_{eff} = \rho_{media} + \left[\left(\frac{M_{ENM} - M_{ENMsol}}{V_{pella}SF}\right)\left(1 - \frac{\rho_{media}}{\rho_{ENM}}\right)\right] \quad (1)$$

where ρ_{media} is the density of the media (g/cm^3), M_{ENM} is the total mass of ENMs (g) in the dispensed volume (1 ml) of suspension, M_{ENMsol} is the mass of dissolved ENMs (g) in the dispensed volume of suspension. The final ρ_{eff} was calculated as the average of the three values.

Fate and transport modeling for calculation of dose delivered to cells—The distorted grid (DG) model reported by DeLoid et al. (DeLoid et al., 2015). was utilized to calculate the concentration profiles across the well of a 96-well plate, the concentration at the bottom of the well (bottom concentration), and the fraction of deposited particles to the cell surface as a function of the exposure time (f_D) for the nanoparticle suspension. The developed code was executed on MATLAB (MathWorks, Massachusetts, USA). Inputs for the model were the agglomerate volume-weighted hydrodynamic diameter (d_H) and ρ_{eff} of ENM agglomerates suspended in RPMI+10%(vol/vol) FBS. For more details, the readers are referred to the above reference (DeLoid et al., 2015).

Empirical mathematical equations for calculating concentration and fraction delivered to cell as a function of exposure time—While validated computational models, such as the DG model, are available to nanotoxicologists to perform ultimately accurate estimates for delivered-to-cell dose metrics, empirical approaches through relevant *in-vitro* dose (RID) functions can be alternatively used to avoid cumbersome repetitions of sophisticated fate and transport numerical algorithms (Pal et al., 2015a, 2015b). To do so, the ENM concentration at the cell-medium interface (C_{CMI}) from the DG model was normalized with respect to the administered dose (C_{Adm}). The normalized concentration at cell-medium

interface (C_{Norm}) is a unitless quantity. The Levenberg–Marquardt algorithm was used to fit the C_{Norm} with a semi-empirical modified exponential function:

$$C_{Norm}\left(t\right) = C_0 + \alpha\left(1 - e^{-t/\tau_1}\right), \quad (2)$$

where C_0 is the normalized concentration at cell-medium interface at t=0 and a is a unitless constant, while τ is in hrs. Assuming that the ENM suspension has been prepared following the present protocol and the DLS and effective density data are in agreement with those displayed here, the following equation can be used to calculate the concentration at a given time point for a specific administered dose as a function of exposure time:

$$C_{CMI}\left(t\right) = C_{Adm}\left[C_0 + \alpha\left(1 - e^{-t/\tau_1}\right)\right], \quad (3)$$

Similarly, the fraction deposited to cell data were fit with the function:

$$F_D\left(t\right) = F_0 + \beta\left(1 - e^{-t/\tau_2}\right), \quad (4)$$

where F_0 is the deposited-to-cell fraction at t=0, β is a unitless constant and τ is in hrs. All constants are material and media specific. Assuming that the ENM suspension has been prepared following the present protocol and the DLS data are in agreement with those displayed here, equation 4 can be used to calculate the fraction delivered to cell at a given time point for such ENM.

Statistics, fitting and error analysis—All measurements in water and RPMI+10%(vol/vol) FBS (test biological medium) were done in triplicate. The average of the triplicates is reported as the measurement value, and the standard deviation is reported as the error of the measurements. The DG curves were fitted using Pro Fit 6.2.16 (Quantum Soft) via the Levenberg-Marquardt algorithm.

3. Results and discussion

A high throughput (volume) and precision flame spray pyrolysis (FSP) approach coupled with state-of-the-art characterization techniques are utilized to generate such reference ENMs. Nine reference metal and metal oxide ENMs with low aspect ratio were synthesized using this in-house developed FSP based approach. The reference ENMs were then characterized to determine their physical, chemical and morphological properties. In addition, potential endotoxin and bacterial contamination were also assessed. Finally, their colloidal properties in water and a test biological medium were characterized, and considerations for cellular dosimetry were provided. In more detail:

3.1. Physicochemical and morphological characterization of generated reference ENMs

Fig. 2a depicts the TEM images of synthesized reference ENMs at different magnifications. Imaging analysis indicates that the chain-like agglomerates/aggregates of ENMs consist of smaller primary particles, which is typical in FSP-synthesized nanomaterials (Teleki et al., 2008; Teoh et al., 2010; Wegner et al., 2003; Strobel et al., 2007; De Temmerman et al., 2012, 2014; Verleysen et al., 2014). In addition, the ENMs exhibit relatively narrow primary particle size distributions (see Fig. S1) following a log-normal distribution with geometric standard deviations between 1.3 and 1.6, which is also in agreement with published data for flame-generated ENMs (Teleki et al., 2008; Teoh et al., 2010; Wegner et al., 2003; Strobel et al., 2007). The TEM size results were confirmed with the SSA measurements (Table 1). In addition, three shape factors (aspect ratio, circularity and roundness) of the ENMs were analyzed and outlined in Table 2, which indicate that the ENMs are near spherical (other than ceria) and exhibit smooth surfaces without detectable roughness.

The XRD patterns of ENMs are depicted in Fig. 2b. The crystallite size of each ENMs was determined by the Scherrer's formula and summarized in Table 1. Most of the ENMs were found to be in single phase in accordance with literature (Teoh et al., 2010; Levin et al., 1998; Kim et al., 2004; McPherson et al., 1980) with variable degree of crystallinity. This was further confirmed by selected area electron diffraction (SAED) analysis. The exception was alumina, which is composed of two mixed phases (52% monoclinic θ-alumina and 48% orthorhombic δ^*-alumina) (Beltran-Huarac et al., 2014a, 2014b), which is consistent with reports that state that the residence time for growing single-phase crystals is too short for refractory ENMs, such as alumina. However, it should be noted that FSP 30nm Al_2O_3 is a good representation of alumina powders produced commercially, which have mixed-crystal phases and are polycrystalline (Phung et al., 2014).

Table 2 summarizes the pore size analysis that includes the total pore volume (TPV) and average pore size (APS) of ENMs. Since TEM imaging for all ENMs did show the presence of pores and the fact that the detection limit of BET instrument for pores is 2 nm, the pore volume is associated to the inter-particle spacing, which is closely related to the packing factor. The raw density values of ENMs are listed in Table 2. For most ENMs, the density of nanostructured metal oxides was similar to their bulk counterparts. Lower values can be attributed to both the nanoscale nature of ENMs (Nanda et al., 2012) and their mixed crystal structure (Levin et al., 1998).

Fig. S2 depicts the XPS survey spectra of ENMs. The binding energy peaks were ascribed to the core metal electron transitions and metal and oxygen transitions in ENMs. The elemental concentration analysis is summarized in Table S2. The stoichiometry of ENMs calculated upon direct extrapolation of the atomic contents of elements is listed in Table 3, whereof only small variations (≤10%) when compared to its ideal values were observed for most ENMs. The measured carbon contents for most ENMs are below 14%. Carbon is surface bound and comes from the traces of residual organic carbon during the synthesis process or from the short exposure of the ENMs in the air during sample preparation. However, since XPS is a technique sensitive to surface (penetration depth ~5 nm) it is biasing the carbon value. It is also worthy of remark that the XPS carbon levels for our reference ENMs are

significantly lower than those typically observed in flame-generated ENMs (Gass et al., 2013) due in part to the storage of ENMs in argon.

XPS results were confirmed with the more precise EC/OC analysis (see Table 3). As expected, no significant presence of elemental carbon was detected (the levels were below 0.02% for all ENMs). The organic carbon content of up to 0.5% correlates well with the XPS data, which also showed traces of surface carbon, and is lower than those reported (*ca.* 10%) using sol-gel synthesis (Braziulis et al., 2014). The carbon is at very low levels and in its majority, is organic carbon that comes from residual organics produced during FSP process. Note that organic solvents and metalorganic alkoxides are employed to generate metals and metal oxides. It is quite common to obtain traces of organic forms of carbon in flame synthesis. Here all the recipes were optimized by increasing the oxygen supply and achieving complete combustion of the organics. The low level of carbon content is ascribed to the high-temperature profile used during synthesis, which enables the combustion of all organics (Pratsinis 1998), but more importantly, to the fine-tuning of the spray/flame parameters during the optimization of synthesis that effectively eliminated the presence of organic species. Furthermore, the storage under Ar atmosphere was of paramount importance to keep those levels low through the post production phase, as organics can be adsorbed from ambient air.

ICP-MS results including trace metal analysis, metal elemental masses, elemental carbon and oxygen contents and stoichiometry of ENMs are outlined in Table 3 and Table S2. It should be noted that ICP-MS instrument detected more than 50 trace elements. Trace metal analysis showed that all ENMs exhibit metals purity above 99.9% (except for silver 99.0%), as shown in Table 3, and in agreement with the values reported in the literature for FSP-synthesized ENMs (Strobel et al., 2007; Teoh et al., 2010; Pratsinis 1998). The weight (w/w) ratios of silver to silica for 3.5%Ag-SiO_2 and 15%Ag-SiO_2 were 3.79±0.08% and 15.92±0.25%, respectively, consistent with the theoretical expectations (4.7% and 16.7%, respectively). The stoichiometry values of ENMs calculated following a mass balance method showed small variations (see Table 3), when compared to their ideal values. However, for stoichiometry calculations, XPS is more reliable since it directly measures the metals and oxygen atomic ratios, as compared to ICP-MS that measures only metals and relies on the closing of the mass balance to calculate stoichiometric ratios.

FTIR spectra of ENMs are depicted in Fig. S3. The relatively-broad low-frequency vibrational bands were attributed to the metal-oxygen stretching modes of ENMs in the range of 1250–500 cm^{-1}. Specifically, the absorption bands correspond to the stretching of partially occupied metal cations against oxygen (Thapa et al., 2017; Rojas-Perez et al., 2015), and characteristic of vacancy ordering in ENMs. No silver-oxygen stretching mode was detected for 20nm silver, which indicates the absence of significant amounts of AgO or AgO_2. It is noteworthy that ENMs show no significant stretch of carbon-oxygen and carbon-hydrogen bonds. The exception was ceria that shows slight traces of inorganic carbonate stemming from the absorbed CO_2, which is in agreement with literature (Wallace et al., 2013) and the OC data that indicated that ceria exhibits the highest level of OC. The formation of minor surface carbonates in ceria is likely attributed to the exposure of ceria to CO_2 during the synthesis. No substantial O-H stretch was observed in ENMs (except in

10nm ceria wherein a less-intense broad band was detected), *i.e*, ENM surfaces were almost-free of detectable moisture (Diaz-Diestra et al., 2017). From these results, it can be stated that the reference ENMs possess no detectable surface functional groups onto their neutral and partially-charged surface. Surface chemistry of ENMs is critical to delineate the functional properties of protein corona formation with potential implications in dose metrics.

Taken altogether, VENGES platform is ideal for producing highly stoichiometric and pure (99.97%) metals and metal oxides suitable for nanotoxicology research. Their purity extends beyond the purity of the metal oxide to the content of EC and OC, which was minimal. Typically, flame-generated nanomaterials have elemental carbon in the form of soot, which is ascribed to the incomplete combustion (Teoh et al., 2010; Pratsinis 1998). However, all the carbon found on ENM surfaces was found to be organic, and was attributed to the brief exposure to ambient air during *ex-situ* characterization procedures. These findings were further confirmed with XPS and FTIR analyses. This is an important component in synthesis of reference ENMs since carbon can interfere with toxicological studies.

These physicochemical and morphological characterization results collectively highlight VENGES's ability to produce reference ENMs in high volume and with controlled properties. In addition, the ENMs have a smooth surface with no observable pores. It is worth noting that compared to other synthesis methods (such as wet chemical), FSP does not produce monodisperse nanoparticles. Nevertheless, wet synthesis methods have other drawbacks, including high-level usage of organics, high levels of organics on their surface, suspensions at relatively low concentration (typically around 50 μg/ml), and typically low yields (mg/h), rendering them non-cost-effective to produce high volumes needed for *in-vitro* and inhalation toxicological studies.

It is also worth mentioning that the developed FSP based platform in addition to its evidenced ability to produce a variety of metal/metal oxides, it can also be used to synthesize a broad family of bimetallic ENMs, such as Al_2O_3/TiO_2, V_2O_5/TiO_2 and V_2O_5/Al_2O_3, and SiO_2-based composites, iron embedded in SiO_2, TiO_2/SiO_2, SiO_2/GeO_2 and carbon-SiO_2 (Kammler et al., 2001; Stark et al., 2002). Furthermore, an in-line SiO_2 coating reactor can allow for hermetical encapsulations of ENMs with a nanothin layer of amorphous SiO_2 (Gass et al., 2013; Sotiriou et al., 2011, 2014). Such safer-by-design SiO2 coating approach has been shown effective for some ENMs (ZnO, CeO2 and Ag) to significantly lower toxic responses, *e.g.* low damage to DNA when compared to uncoated cores or bare ENMs both in-vitro (Gass et al., 2013; Sotiriou et al., 2014) and in-vivo (Demokritou et al., 2013; Konduru 2015, 2016).

3.2. Endotoxin Levels and bacterial assessment

The results of endotoxin and bacterial characterization are summarized in Table 3. The endotoxin levels of ENM (other than 15% silver supported on silica) suspension prepared at 0.1 mg/ml were below the limit of detection and below the acceptable limit of 0.5 EU/ml. Further, those values are well below the PBS (reportedly to have up to 76 EU/ml) and FBS, values both widely used in cell culture or airborne particulate toxicological studies (Gorbet et al., 2005; Guo et al., 2009; Kirikae et al., 1997; Rylander et al., 1984; Vetten et al., 2014). It is worth noting that the endotoxin levels in FSP-made ENMs were expected to be low due

to the high-temperature conditions used during synthesis, which facilitates the complete combustion of all organic molecules. Albeit endotoxin characterization is a parameter often ignored during synthesis of ENMs; however, endotoxin presence can introduce a significant bias in biological assessment of ENMs (Li et al., 2016). Therefore, for reference ENMs, it is imperative to characterize the endotoxins and make sure that reference ENMs have endotoxin levels within the acceptable levels.

In addition, bacterial assessment indicated no presence of bacteria as shown in Table 3. It should be noted that the harsh flame conditions within the FSP chamber and the aseptic techniques used and the storage under argon environment facilitated the removal of all water and oxygen traces, and minimize any bacteria contamination.

3.3. Suspension preparation, colloidal characterization and cellular dosimetric analysis of ENMs

Even though the powder-derived physical, morphological and chemical properties of ENMs were accurately ascertained by state-of-the-art characterization techniques, such results are not sufficient to predict neither the bioactivity of metals and metal oxides nor their fate and transport in environmental and biological media, which are influenced by the extrinsic properties of the media and suspension preparation methods. For instance, in this study, a test biological media (RPMI + 10% (vol/vol) FBS) was used to evaluate the ENM transformations in biological media and the implications for *in-vitro* dosimetry (DeLoid 2015). Same methodology can be used for biological/culture media of interest.

The critical delivered sonication energy (DSE_{cr}) and the type of sonication used to disperse the ENMs in DI water and RPMI + 10% (vol/vol) FBS along with their colloidal properties are summarized in Table S3. From this Table, it is noted that 20nm silver, 15% silver supported on silica, 10nm ceria and 100nm iron oxide underwent a fast settling, and therefore a discrete sonication approach was followed to effectively disperse them in DI water. At 24 hours after dispersion in the medium, the mean volume-weighted sizes and mean PDI values did not show any statistically significant change (other than for alumina and 15% silver supported on silica having a 13–17% change in size), which indicates that the formed ENM agglomerates were stable over 24 hours in the medium. As expected, the mean effective density values of ENM agglomerates determined by VCM method turned out to be significantly lower than those listed in Table 2 for pristine dry ENMs. The values varied from 0.13 g/cc for silica to 2.16 g/cc for silver. See Table S3 for more details on the colloidal properties of ENMs.

The mean effective density values and volume-weighted size distributions for formed agglomerates in the test biological medium were used to calculate the dose metrics through the DG model. Table S4 lists the main fate and transport modeling parameters (automatically generated by the simulation) that includes the mean delivered-to-cell mass concentration and fraction deposited of ENMs dispersed in RPMI + 10% (vol/vol) FBS at 6, 12 and 24 hours. The absolute values of the normalized delivered-to-cell mass concentrations and fractions deposited as a function of the exposure time are plotted in Fig. 3 and Fig. S4. From these results, it is inferred that ENMs were well-dispersed in the biological medium and the agglomerates settle gradually to reach the maximum concentration at the bottom of the well

and fraction deposited at 24 hours (except 100nm iron oxide that reached a mean concentration as high as 24 mg/ml at 3 hours). It was observed that, in general, ENMs having greater values for both agglomerate size and effective density deposited more rapidly than those with smaller values for both properties, as expected (Cohen et al., 2014a). Our results confirm that the administered and delivered doses vary significantly (from a factor of ~3 to 60, and up to ~300 for 100nm iron oxide, at 24 hours) depending on the media and material, accentuate the importance of characterizing ENM-suspensions for both effective density and agglomerate size, and include dosimetric considerations in cellular studies.

Further, it was also found that it takes 6 hours to deposit 81% of the administered dose for 100nm iron oxide, and takes long 24 hours to deposit only an insignificant 0.7% of the administered dose for 3.5% silver supported on silica. It is thus clear that ENM-ENM and ENM-media interactions, and the way how ENMs agglomerates settle and diffuse in media, affect profoundly the effective dose that cells receive at the bottom of the well. Moreover, ENM bioactivity differs in relation to their physical, morphological and chemical properties and surface chemistry. Differences in delivered to cell dose values provide challenges to compare dose-response curves between ENMs with fast and slow transport. Such challenges could be partially addressed by reporting delivered doses *in vitro*, following our integrated methodology (DeLoid et al., 2017), rather than using administered doses which is the common practice in cellular nanotoxicology studies. Nonetheless, more elaborate studies are needed to include potential dissolution of ENMs in biological media. Finally, it should be mentioned that relevant *in-vitro* dose functions can be alternatively used to calculate delivered to cell dose metrics for other exposure time points, and to avoid repetitions of MATLAB code that implies cumbersome numerical algorithms for the same ENM and media conditions. The output plots fitted using equations 2 and 4, and the fitting parameters (that are material- and medium-specific) of this semi-empirical approach can be found in Table S5 for interested readers.

4. Conclusion

Reference metal and metal oxide ENMs were synthesized using a high throughput (yield) and precision platform using an industrially relevant flame spray pyrolysis platform. The large array of highly-pure and property controlled reference ENMs were produced at high volume rates (g/h) and at nanometer precision. VENGES is an ideal platform to synthesize reference ENMs as it enables fine-tuning of the ENM size, composition, crystallinity, stoichiometry and surface chemistry of ENMs. The synthesized ENMs were free of endotoxins and bacteria with low residual of organic carbon onto their surface. As pointed out in this study, physicochemical and morphological characterizations of powder-derived ENMs were not sufficient to predict neither the bioactivity and fate and transport of ENM agglomerates in biological media. It was found that ENM-ENM and ENM-media interactions, and the way how ENMs agglomerates settle in biological media, affect profoundly the effective dose that cells receive. Variability in delivered doses might have potential implications in re-interpreting previously-reported toxicity screens of large panel of ENMs. Finally, the importance of considering the particle dose actually delivered to cells will elucidate the realistic mechanisms, whereby ENMs induce cellular toxicity, and harmonize the validity, consistency and relevance of *in-vitro* toxicity reports.

Supplementary Material

Refer to Web version on PubMed Central for supplementary material.

Acknowledgments

The authors thank Dr. Sandra V. Pirela for fruitful comments on dosimetry data. Special thanks to Ms. Daysi Diaz-Diestra for help on managing and processing the dosimetry data.

Funding information

Research reported in this publication was supported by the HSPH Center for Nanotechnology and Nanotoxicology and National Institute of Environmental Health Sciences under Award Number (NIH grant # U24ES026946). The content is solely the responsibility of the authors and does not necessarily represent the official views of the National Institutes of Health. The engineered nanomaterials used in the research presented in this publication have been procured/synthesized, characterized, and provided by the Engineered Nanomaterials Resource and Coordination Core established at Harvard T. H. Chan School of Public Health (NIH grant # U24ES026946) as part of the Nanotechnology Health Implications Research (NHIR) Consortium. This research was supported in part by an appointment to the Research Participation Program at the U.S. Air Force Research Laboratory, 711 Human Performance Wing, Human Effectiveness Directorate, Bioeffects Division, Molecular Bioeffects Branch administered by the Oak Ridge Institute for Science and Education through an interagency agreement between the U.S. Department of Energy and USAFRL. This work was performed in part at the Harvard University Center for Nanoscale Systems (CNS), a member of the National Nanotechnology Coordinated Infrastructure Network (NNCI), which is supported by the National Science Foundation under NSF ECCS award no. 1541959.

References

Barrett EP, Joyner LG, Halenda PP. The Determination of Pore Volume and Area Distributions in Porous Substances. I. Computations from Nitrogen Isotherms. J. Am. Chem. Soc. 1951; 73:373–380. (Available: http://pubs.acs.org/doi/abs/10.1021/ja01145a126).

Beauchemin D. Inductively Coupled Plasma Mass Spectrometry. Anal. Chem. 2010; 282:4786–4810. (Available: http://pubs.acs.org/doi/abs/10.1021/ac101187p).

Bello D, Martin J, Santeufemio C, Sun Q, Lee BK, Shafer M, et al. Physicochemical and morphological characterisation of nanoparticles from photocopiers: implications for environmental health. Nanotoxicology. 2013; 7:989–1003. DOI: 10.3109/17435390.2012.689883 [PubMed: 22551088]

Beltran-Huarac J, Palomino J, Resto O, Wang J, Jadwisienczak WM, Weiner BR, et al. Highly-crystalline γ-MnS nanosaws. RSC Adv. 2014a; 4:38103–38110. (Available: http://pubs.rsc.org/en/Content/ArticleLanding/2014/RA/c4ra05561f#!divAbstract).

Beltran-Huarac J, Resto O, Carpena-Nunez J, Jadwisienczak WM, Fonseca LF, Weiner BR, et al. Single-crystal γ-MnS nanowires conformally coated with carbon. ACS Appl. Mater. Interfaces. 2014b; 6:1180–1186. (Available: http://pubs.acs.org/doi/abs/10.1021/am404746k). [PubMed: 24392737]

Bish DL, Howard SA. Quantitative phase analysis using the Rietveld method. J. Appl. Cryst. 1988; 21:86–91. DOI: 10.1107/S0021889887009415

Braziulis G, Janulevicius G, Stankeviciute R, Zalga A. Aqueous sol–gel synthesis and thermoanalytical study of the alkaline earth molybdate precursors. J. Therm. Anal. Calorim. 2014; 118:613–621. (Available: https://link.springer.com/article/10.1007/s10973-013-3579-0).

Burnett DJ, Heng JYY, Thielmann F, Garcia AR, Naderi M, Acharya M. Measuring Surface Roughness of Pharmaceutical Powders Using Vapor Sorption Methods. AAPS PharmSciTech. 2010; 12:56–61. (Available: https://www.ncbi.nlm.nih.gov/pmc/articles/PMC3066367/). [PubMed: 21170618]

Chalbot M-C, , Pirela SV, , Schifman M, , Kasaraneni V, , Craver VO, , Bello D. , et al. Synergistic effects of engineered nanoparticles and organics released from laser printers using nano-enabled toners: From exposures to the emitted organic aerosol. Environ. Sci.: Nano accepted manuscript 2017 (Available: http://pubs.rsc.org/en/content/articlelanding/2017/en/c7en00573c#!divAbstract)

Cohen J, DeLoid G, Pyrgiotakis G, Demokritou P. Interactions of engineered nanomaterials in physiological media and implications for in vitro dosimetry. Nanotoxicology. 2013; 7:417–431. DOI: 10.3109/17435390.2012.666576 [PubMed: 22393878]

Cohen JM, Teeguarden JG, Demokritou P. An integrated approach for the in vitro dosimetry of engineered nanomaterials. Part. Fibre Toxicol. 2014a; 11:20. (Available: https://particleandfibretoxicology.biomedcentral.com/articles/10.1186/1743-8977-11-20). [PubMed: 24885440]

Cohen JM, Derk R, Wang L, Godleski J, Kobzik L, Brain J, et al. Tracking translocation of industrially relevant engineered nanomaterials (ENMs) across alveolar epithelial monolayers in vitro. Nanotoxicology. 2014b; 8:1–10. DOI: 10.3109/17435390.2013.879612 [PubMed: 23092443]

Cohen JM, DeLoid GM, Demokritou P. A critical review of in vitro dosimetry for engineered nanomaterials. Nanomedicine. 2015; 10:3015–3032. (Available: http://www.futuremedicine.com/doi/abs/10.2217/nnm.15.129?journalCode=nnm). [PubMed: 26419834]

Cohen JM, Beltran-Huarac J, Pyrgiotakis G, Demokritou P. Effective delivery of sonication energy to fast settling and agglomerating nanomaterial suspensions for cellular studies: Implications for stability, particle kinetics, dosimetry and toxicity. NanoImpact in revision. 2017

DeLoid GM, Cohen JM, Pyrgiotakis G, Pirela SV, Pal A, Liu G, et al. Advanced computational modelling for in vitro nanomaterial dosimetry. Part. Fibre Toxicol. 2015; 12:32. (Available: https://particleandfibretoxicology.biomedcentral.com/articles/10.1186/s12989-015-0109-1). [PubMed: 26497802]

DeLoid G, Casella B, Pirela S, Filoramo R, Pyrgiotakis G, Demokritou P, et al. Effects of engineered nanomaterial exposure on macrophage innate immune function. NanoImpact. 2016; 2:70–81. DOI: 10.1016/j.impact.2016.07.001 [PubMed: 29568809]

DeLoid GM, Cohen JM, Pyrgiotakis G, Demokritou P. Preparation, characterization, and in vitro dosimetry of dispersed, engineered nanomaterials. Nat. Protoc. 2017; 12:355–371. (Available: https://www.nature.com/nprot/journal/v12/n2/full/nprot.2016.172.html). [PubMed: 28102836]

Demokritou P, Buchel R, Molina RM, DeLoid G, Brain JD, Pratsinis SE. Development and characterization of a Versatile Engineered Nanomaterial Generation System (VENGES) suitable for toxicological studies. Inhalation Toxicol. 2010; 22:107–116. DOI: 10.3109/08958378.2010.499385

Demokritou P, Gass S, Pyrgiotakis G, Cohen JM, Goldsmith W, McKinney W, et al. An in vivo and in vitro toxicological characterisation of realistic nanoscale CeO2 inhalation exposures. Nanotoxicology. 2013; 7:1338–1350. DOI: 10.3109/17435390.2012.739665 [PubMed: 23061914]

De Temmerman P-J, Lammertyn J, De Ketelaere B, Kestens V, Roebben G, Verleysen E, Mast J. Measurement uncertainties of size, shape, and surface measurements using transmission electron microscopy of near-monodisperse, near-spherical nanoparticles. J. Nanopart. Res. 2014; 16:2177.doi: 10.1007/s11051-013-2177-1

De Temmerman P-J, Van Doren E, Verleysen E, Van der Stede Y, Francisco MAD, Mast J. Quantitative characterization of agglomerates and aggregates of pyrogenic and precipitated amorphous silica nanomaterials by transmission electron microscopy. J. Nanobiotech. 2012; 10:24.doi: 10.1186/1477-3155-10-24

Diaz-Diestra D, Thapa B, Beltran-Huarac J, Weiner BR, Morell G. L-cysteine capped ZnS:Mn quantum dots for room-temperature detection of dopamine with high sensitivity and selectivity. Biosens. Bioelectron. 2017; 87:693–700. DOI: 10.1016/j.bios.2016.09.022 [PubMed: 27631684]

El Badawy AM, Luxton TP, Silva RG, Scheckel KG, Suidan MT, Tolaymat TM. Impact of environmental conditions (pH, ionic strength, and electrolyte type) on the surface charge and aggregation of silver nanoparticles suspensions. Environ. Sci. Technol. 2010; 44:1260–1266. (Available: http://pubs.acs.org/doi/abs/10.1021/es902240k). [PubMed: 20099802]

Eleftheriadou M, Pyrgiotakis G, Demokritou P. Nanotechnology to the rescue: Using nano-enabled approaches in microbiological food safety and quality. Curr. Opin. Biotechnol. 2017; 44:87–93. DOI: 10.1016/j.copbio.2016.11.012 [PubMed: 27992831]

Gass S, Cohen JM, Pyrgiotakis G, Sotiriou GA, Pratsinis SE, Demokritou P. A safer formulation concept for flame-generated engineered nanomaterials. ACS Sustainable Chem. Eng. 2013; 1:843–857. (Available: http://pubs.acs.org/doi/abs/10.1021/sc300152f%40proofing). [PubMed: 23961338]

Glover RD, Miller JM, Hutchison JE. Generation of metal nanoparticles from silver and copper objects: nanoparticle dynamics on surfaces and potential sources of nanoparticles in the environment. ACS Nano. 2011; 5:8950–8957. (Available: http://pubs.acs.org/doi/abs/10.1021/nn2031319). [PubMed: 21985489]

Gorbet MB, Sefton MV. Endotoxin: The uninvited guest. Biomaterials. 2005; 26:6811–6817. DOI: 10.1016/j.biomaterials.2005.04.063 [PubMed: 16019062]

Grant JT. Methods for quantitative analysis in XPS and AES. Surf. Interface Anal. 1989; 14:271–283. (Available: http://onlinelibrary.wiley.com/doi/10.1002/sia.740140602/abstract).

Guo B, Zebda R, Drake SJ, Sayes CM. Synergistic effect of co-exposure to carbon black and Fe_2O_3 nanoparticles on oxidative stress in cultured lung epithelial cells. Part. Fibre Toxicol. 2009; 6:4. (Available: https://link.springer.com/article/10.1186/1743-8977-6-4). [PubMed: 19203368]

ISO Guide. Terms and definitions used in connection with reference materials. 1992; 30 Available: https://www.iso.org/standard/21638.html.

ISO/Guide 30. Reference materials — Selected terms and definitions 2015 Available: https://www.iso.org/obp/ui/#iso:std:iso:guide:30:ed-3:v1:en

ISO/IEC Guide. International vocabulary of metrology - Basic and general concepts and associated terms (VIM). 2007; 99 Available: https://www.iso.org/obp/ui/#iso:std:iso-iec:guide:99:ed-1:v2:en.

Izak-Nau E, Huk A, Reidy B, Uggerud H, Vadset M, Eiden S, et al. Impact of storage conditions and storage time on silver nanoparticles' physicochemical properties and implications for their biological effects. RSC Adv. 2015; 5:84172–84185. (Available: http://pubs.rsc.org/en/Content/ArticleLanding/2015/RA/c5ra10187e#!divAbstract).

Kammler HK, Mädler L, Pratsinis SE. Flame Synthesis of Nanoparticles. Chem. Eng. Technol. 2001; 24:583–596. (Available: http://onlinelibrary.wiley.com/doi/10.1002/15214125(200106)24:6%3C583::AID-CEAT583%3E3.0.CO;2-H/abstract).

Keller AA, McFerran S, Lazareva A, Suh S. Global life cycle releases of engineered nanomaterials. J. Nanopart. Res. 2013; 15:1692. (Available: https://link.springer.com/article/10.1007/s11051-013-1692-4).

Kim S, Gislason JJ, Morton RW, Pan XQ, Sun HP, Laine RM. Liquid-feed flame spray pyrolysis of nanopowders in the alumina−titania system. Chem. Mater. 2004; 16:2336–2343. (Available: http://pubs.acs.org/doi/abs/10.1021/cm0497531).

Kirikae T, Tamura H, Hashizume M, Kirikae F, Uemura Y, Tanaka S. Endotoxin contamination in fetal bovine serum and its influence on tumor necrosis factor production by macrophage-like cells J774.1 cultured in the presence of the serum. Int. J. Immunopharmacol. 1997; 19:255–262. DOI: 10.1016/S0192-0561(97)00066-0 [PubMed: 9439764]

Konduru NV, Jimenez RJ, Swami A, Friend S, Castranova V, Demokritou P, et al. Silica coating influences the corona and biokinetics of cerium oxide nanoparticles. Part. Fibre Toxicol. 2015; 12:31.doi: 10.1186/s12989-015-0106-4 [PubMed: 26458946]

Konduru NV, Murdaugh KM, Swami A, Jimenez RJ, Donaghey TC, Demokritou P, et al. Surface modification of zinc oxide nanoparticles with amorphous silica alters their fate in the circulation. Nanotoxicology. 2016; 10:720–727. DOI: 10.3109/17435390.2015.1113322 [PubMed: 26581431]

Levin I, Brandon D. Metastable alumina polymorphs: Crystal structures and transition sequences. J. Am. Chem. Soc. 1998; 81:1995–2012. (Available: http://onlinelibrary.wiley.com/doi/10.1111/j.1151 2916.1998.tb02581.x/abstract).

Li Y, Boraschi D. Endotoxin contamination: a key element in the interpretation of nanosafety studies. Nanomedicine. 2016; 11:269–287. (Available: http://www.futuremedicine.com/doi/abs/10.2217/nnm.15.196). [PubMed: 26787429]

McClements DJ, DeLoid G, Pyrgiotakisb G, Shatkinc JA, Xiaoa H, Demokritou P. The role of the food matrix and gastrointestinal tract in the assessment of biological properties of ingested engineered nanomaterials (iENMs): State of the science and knowledge gaps. NanoImpact. 2016; 3–4:47–57. DOI: 10.1016/j.impact.2016.10.002

McPherson R. On the formation of thermally sprayed alumina coatings. J. Mater. Sci. 1980; 15:3141–3149. (Available: https://link.springer.com/article/10.1007/BF00550387).

Molina RM, Konduru NV, Jimenez RJ, Pyrgiotakis G, Demokritou P, Wohlleben W, et al. Bioavailability, distribution and clearance of tracheally instilled, gavaged or injected cerium

dioxide nanoparticles and ionic cerium. Environ. Sci.: Nano. 2014; 1:561–573. (Available: http://pubs.rsc.org/en/content/articlelanding/2014/en/c4en00034j#!divAbstract).

Monecke T, Köhle,r S, Kleeberg R, Herzig PM, Gemmell JB. Quantitative phase-analysis by the Rietveld method using x-ray powder-diffraction data: Application to the study of alteration halos associated with volcanic-rock-hosted massive sulfide deposits. The Canadian Mineralogist. 2001; 39:1617–1633. (Available: http://www.canmin.org/content/39/6/1617.abstract).

Nanda KK. Size-dependent density of nanoparticles and nanostructured materials. Phys. Lett. A. 2012; 376:3301–3302. DOI: 10.1016/j.physleta.2012.10.001

Oostingh GJ, Casals E, Italiani P, Colognato R, Stritzinger R, Ponti J, et al. Problems and challenges in the development and validation of human cell-based assays to determine nanoparticle induced immunomodulatory effects. Part. Fibre Toxicol. 2011; 8:8. (Available: https://particleandfibretoxicology.biomedcentral.com/articles/10.1186/1743-8977-8-8). [PubMed: 21306632]

Orts-Gil g, Natte K, , Österle W. Multi-parametric reference nanomaterials for toxicology: state of the art, future challenges and potential candidates. RSC Adv. 2013; 3:18202–18215. (Available: http://pubs.rsc.org/en/content/articlelanding/2013/ra/c3ra42112k#!divAbstract).

Pal AK, Bello D, Cohen, Demokritou P. Implications of in vitro dosimetry on toxicological ranking of low aspect ratio engineered nanomaterials. Nanotoxicology. 2015a; 9:871–885. DOI: 10.3109/17435390.2014.986670 [PubMed: 25672815]

Pal AK, Watson CY, Pirela SV, Singh D, Chalbot M-CG, Kavouras I, et al. Linking exposures of particles released from nano-enabled products to toxicology: An integrated methodology for particle sampling, extraction, dispersion, and dosing. Toxicol. Sci. 2015b; 146:321–333. DOI: 10.1093/toxsci/kfv095 [PubMed: 25997654]

Petersen EJ, Henry TB, Zhao J, MacCuspie RI, Kirschling TL, Dobrovolskaia MA. Identification and avoidance of potential artifacts and misinterpretations in nanomaterial ecotoxicity measurements. Environ. Sci. Technol. 2014; 48:4226–4246. DOI: 10.1021/es4052999 [PubMed: 24617739]

Phung TK, Lagazzo A, Rivero MA, Sánchez V, Busca G. A study of commercial transition aluminas and of their catalytic activity in the dehydration of ethanol. J. Catal. 2014; 311:102–113. DOI: 10.1016/j.jcat.2013.11.010

Pirela SV, Miousse IR, Lu X, Castranova V, Thomas T, Qian Y. Effects of laser printer emitted engineered nanoparticles on cytotoxicity, chemokine expression, reactive oxygen species, DNA methylation, and DNA damage: A comprehensive in vitro analysis in human small airway epithelial cells, macrophages, and lymphoblasts. Environ Health Perspect. 2016a; 124:210–219. DOI: 10.1289/ehp.1409582 [PubMed: 26080392]

Pirela SV, Lu X, Miousse I, Sisler JD, Qian Y, Guo N, et al. Effects of intratracheally instilled laser printer-emitted engineered nanoparticles in a mouse model: A case study of toxicological implications from nanomaterials released during consumer use. NanoImpact. 2016b; 1:1–8. DOI: 10.1016/j.impact.2015.12.001 [PubMed: 26989787]

Pradhan S, Hedberg J, Blomberg E, Wold S, Wallinder IO. Effect of sonication on particle dispersion, administered dose and metal release of non-functionalized, non-inert metal nanoparticles. J. Nanopart. Res. 2016; 18:285. (Available: https://www.ncbi.nlm.nih.gov/pmc/articles/PMC5034002/pdf/11051_2016_Article_3597.pdf). [PubMed: 27774036]

Pratsinis SE. Flame aerosol synthesis of ceramic powders. Prog. Energy Combust. Sci. 1998; 24:197–219. DOI: 10.1016/S0360-1285(97)00028-2

Pyrgiotakis G, Blattmann CO, Pratsinis S, Demokritou P. Nanoparticle-nanoparticle interactions in biological media by atomic force microscopy. Langmuir. 2013; 29:11385–11395. (Available: http://pubs.acs.org/doi/abs/10.1021/la4019585). [PubMed: 23978039]

Pyrgiotakis G, McDevitt J, Bordini A, Diaz E, Molina R, Watson C, et al. A chemical free, nanotechnology-based method for airborne bacterial inactivation using engineered water nanostructures. Environ. Sci.: Nano. 2014a; 1:15–26. DOI: 10.1016/j.jmatprotec.2005.06.053

Pyrgiotakis G, Blattmann CO, Demokritou P. Real-time nanoparticle–cell interactions in physiological media by atomic force microscopy. ACS Sustainable Chem. Eng. 2014b; 2:1681–1690. (Available: http://pubs.acs.org/doi/abs/10.1021/sc500152g). [PubMed: 25068097]

Pyrz WD, Buttrey DJ. Particle size determination using TEM: A discussion of image acquisition and analysis for the novice microscopist. Langmuir. 2008; 24:11350–11360. (Available: http://pubs.acs.org/doi/abs/10.1021/la801367j). [PubMed: 18729338]

Roco MC, Mirkin CA, Hersam MC. Nanotechnology research directions for societal needs in 2020: summary of international study. J. Nanopart. Res. 2011; 13:897–919. (Available: http://www.springer.com/us/book/9789400711679).

Rojas-Perez A, Diaz-Diestra D, Frias-Flores CB, Beltran-Huarac J, Das KC, Weiner BR. Catalytic effect of ultrananocrystalline Fe3O4 on algal bio-crude production *via* HTL process. Nanoscale. 2015; 7:17664–17671. (Available: http://pubs.rsc.org/en/Content/ArticleLanding/2015/NR/c5nr04404a#!divAbstract). [PubMed: 26465090]

Rylander R, Haglind P. Airborne endotoxins and humidifier disease. Clin. Allergy. 1984; 14:109–112. (Available: http://onlinelibrary.wiley.com/doi/10.1111/j.1365-2222.1984.tb02197.x/full). [PubMed: 6697469]

Sandle TA. A Comparative Study of Different Methods for Endotoxin Destruction. Am. Pharmaceut. Rev. 2013; 16:15–17. (Available: http://www.americanpharmaceuticalreview.com/FeaturedArticles/148858-A-Comparative-Study-of-Different-Methods-for-Endotoxin-Destruction/).

Servin AD, White JC. Nanotechnology in agriculture: Next steps for understanding engineered nanoparticle exposure and risk. NanoImpact. 2016; 1:9–12. DOI: 10.1016/j.impact.2015.12.002

Sotiriou GA, Teleki A, Camenzind A, Krumeich F, Meyer A, Panke S, et al. Nanosilver on nanostructured silica: Antibacterial activity and Ag surface area. Chem. Eng. J. 2011; 170:547–554. DOI: 10.1016/j.cej.2011.01.099 [PubMed: 23730198]

Sotiriou GA, Diaz E, Long MS, Godleski J, Brain J, Pratsinis SE, Demokritou P. A novel platform for pulmonary and cardiovascular toxicological characterization of inhaled engineered nanomaterials. Nanotoxicology. 2012; 6:680–690. DOI: 10.3109/17435390.2011.604439 [PubMed: 21809902]

Sotiriou GA, Watson C, Murdaugh KM, Darrah TH, Pyrgiotakis G, Elder A, et al. Engineering safer-by-design silica-coated ZnO nanorods with reduced DNA damage potential. Environ. Sci.: Nano. 2014; 1:144–153. (Available: https://www.ncbi.nlm.nih.gov/pmc/articles/PMC4060637/). [PubMed: 24955241]

Stark WJ, Pratsinis SE. Aerosol flame reactors for manufacture of nanoparticles. Powder Technol. 2002; 126:103–108. DOI: 10.1016/S0032-5910(02)00077-3

Stone V, Nowack B, Baun A, van den Brink N, von der Kammer F, Dusinska M. Nanomaterials for environmental studies: Classification, reference material issues, and strategies for physicochemical characterisation. Sci. Total Environ. 2020; 408:1745–1754. DOI: 10.1016/j.scitotenv.2009.10.035

Strobel R, Pratsinis SE. Flame aerosol synthesis of smart nanostructured materials. J. Mater. Chem. 2007; 17:4743–4756. (Available: http://pubs.rsc.org/en/content/articlelanding/2007/jm/b711652g#!divAbstract).

Taurozzi JS, Hackley VA, Wiesner MR. Ultrasonic dispersion of nanoparticles for environmental, health and safety assessment--issues and recommendations. Nanotoxicology. 2011; 5:711–729. DOI: 10.3109/17435390.2010.528846 [PubMed: 21073401]

Teleki A, Akhtar MK, Pratsinis SE. The quality of SiO2-coatings on flame-made TiO2-based nanoparticles. J. Mater. Chem. 2008; 18:3547–3555. (Available: http://pubs.rsc.org/en/Content/ArticleLanding/2008/JM/b803039a#!divAbstract).

Teoh WY, Amal R, Mädler L. Flame spray pyrolysis: An enabling technology for nanoparticles design and fabrication. Nanoscale. 2010; 2:1324–1347. (Available: http://pubs.rsc.org/en/content/articlelanding/2010/nr/c0nr00017e/unauth#!divAbstract). [PubMed: 20820719]

Thapa B, Diaz-Diestra D, Beltran-Huarac J, Weiner BR, Morell G. Enhanced MRI T_2 relaxivity in contrast-probed anchor-free PEGylated iron oxide nanoparticles. Nanoscale Res. Lett. 2017; 12:312. (Available: https://www.ncbi.nlm.nih.gov/pmc/articles/PMC5407416/). [PubMed: 28454478]

Tsai CS-J, Echevarría-Vega ME, Sotiriou GA, Santeufemio C, Schmidt D, Demokritou P, et al. Evaluation of environmental filtration control of engineered nanoparticles using the Harvard Versatile Engineered Nanomaterial Generation System (VENGES). J. Nanopart. Res. 2012;

14:812–829. (Available: https://link.springer.com/article/10.1007/s11051-012-0812-x). [PubMed: 23412707]

Tsuda A, Konduru NV. The role of natural processes and surface energy of inhaled engineered nanoparticles on aggregation and corona formation. NanoImpact. 2016; 2:38–44. DOI: 10.1016/j.impact.2016.06.002 [PubMed: 29202111]

Verleysen E, De Temmerman P-J, Van Doren E, Francisco MAD, Mast J. Quantitative characterization of aggregated and agglomerated titanium dioxide nanomaterials by transmission electron microscopy. Powder Technol. 2014; 258:180–188. DOI: 10.1016/j.powtec.2014.03.010

Vetten MA, Yah CS, Singh T, Gulumian M. Challenges facing sterilization and depyrogenation of nanoparticles: Effects on structural stability and biomedical applications. Nanomed. Nanotech. Biol. Med. 2014; 10:1391–1399. DOI: 10.1016/j.nano.2014.03.017

Vilanova O, Mittag JJ, Kelly PM, Milani S, Dawson KA, Rädler JO, et al. Understanding the kinetics of protein–nanoparticle corona formation. ACS Nano. 2016; 10:108420–10850. (Available: http://pubs.acs.org/doi/abs/10.1021/acsnano.6b04858).

Wallace R, Brown AP, Brydson R, Wegner K, Milne SJ. Synthesis of ZnO nanoparticles by flame spray pyrolysis and characterization protocol. J. Mater. Sci. 2013; 48:6393–6403. DOI: 10.1007/s10853-013-7439-x

Wang ZL. Transmission electron microscopy of shape-controlled nanocrystals and their assemblies. J Phys. Chem. B. 2000; 104:1153–1175. (Available: http://pubs.acs.org/doi/abs/10.1021/jp993593c).

Watson C, Ge J, Cohen J, Pyrgiotakis G, Engelward BP, Demokritou P. High-Throughput Screening Platform for Engineered Nanoparticle-Mediated Genotoxicity Using CometChip Technology. ACS Nano. 2014; 8:2118–2133. (Available: http://pubs.acs.org/doi/abs/10.1021/nn404871p). [PubMed: 24617523]

Wegner K, Pratsinis SE. Scale-up of nanoparticle synthesis in diffusion flame reactors. Chem. Eng. Sci. 2003; 58:4581–4589. DOI: 10.1016/j.ces.2003.07.010

- Lack of synthesis and characterization of reference engineered nanomaterials for nanotoxicology research.
- High throughput and precision flame spray pyrolysis generates reference metals and metal oxides and enables to precisely control their intrinsic properties.
- Electron microscopy, advanced spectroscopic techniques and physical analyses (*e.g.*, BET, XRD, TEM, pycnometry, XPS, ICP-MS and FTIR) useful to characterize reference nanomaterials.
- FSP metals and metal oxides are of high purity free of bacteria and endotoxins.
- The suitability our recipes & protocols developed in this study are ideal to generate reliable & reproducible toxicological data in an effort to reduce contradicting inter-lab data on their toxicity.

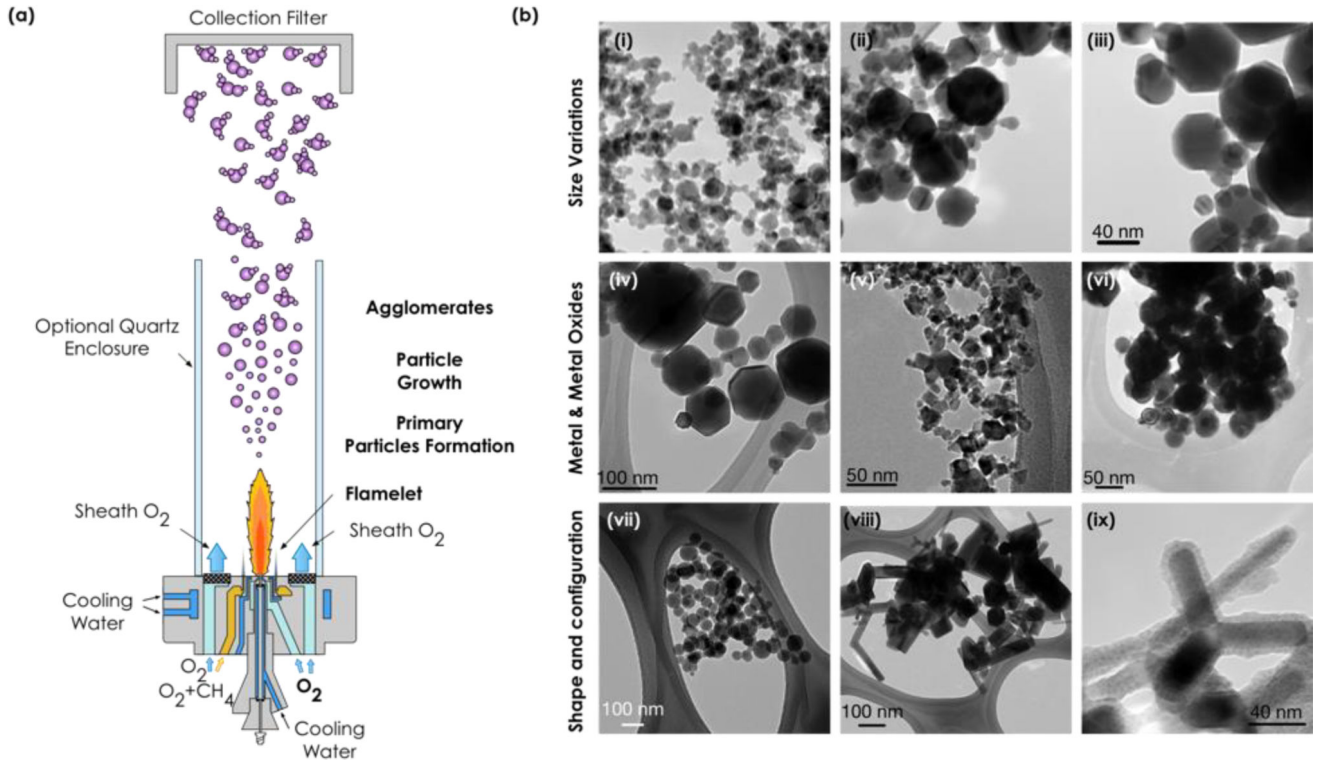

Fig. 1.

(a) Schematic diagram of the Harvard versatile engineered nanomaterials generation system (VENGES) used to synthesize ENMs. (b) TEM images showing the capability and versatility of VENGES to produce a myriad of ENMs, not only the family of reference metals and metal oxides presented in this study but also to produce silica-coated ENMs (*i.e.* SiO_2 coated ZnO) with different size, morphology and configuration. (i-iii) Control in size of iron oxide particles (8nm-i, 25nm-ii and 100nm-iii, images taken under same magnification); (iv-vi) control in type of material (iron oxide-iv, cerium oxide-v and silver-vi); and (vii-ix) control in shape and configuration (spherical-vii, rod shaped-viii and silica coated-ix zinc oxide ENMs). Scale bar in Fig. b-iii is the same for Figs b-i and b-ii.

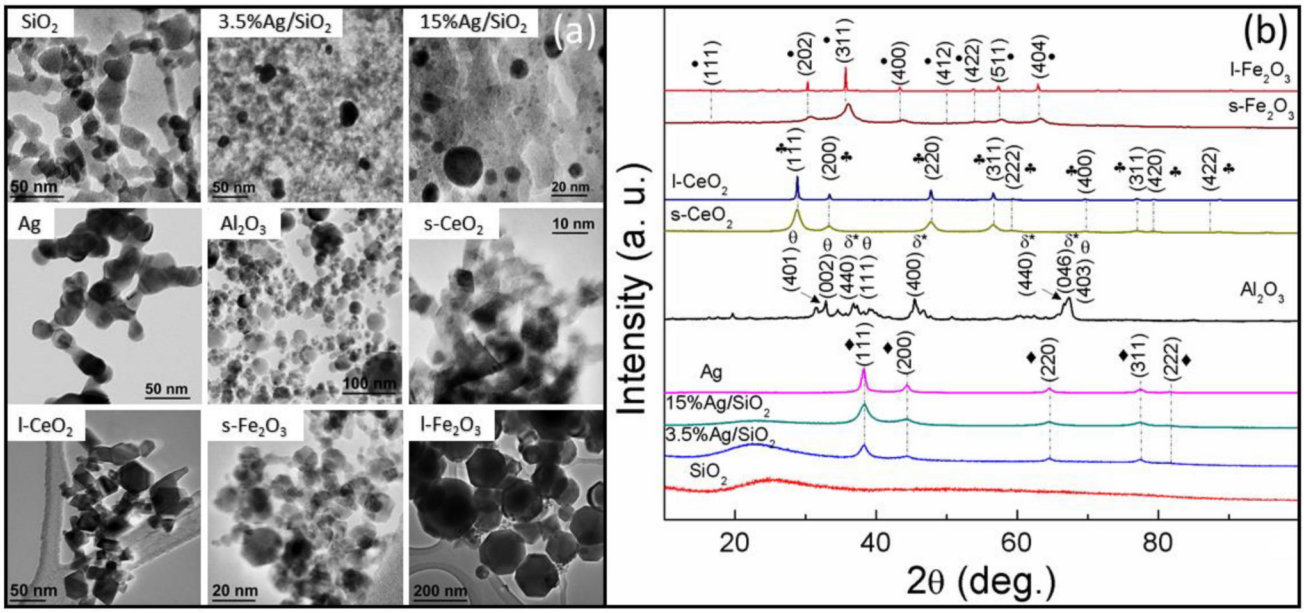

Fig. 2.

(a) Bright field TEM images and (b) XRD patterns and crystallographic indexation of nine ENMs synthesized by flame spray pyrolysis using the Harvard versatile engineered nanomaterials generation system (VENGES).

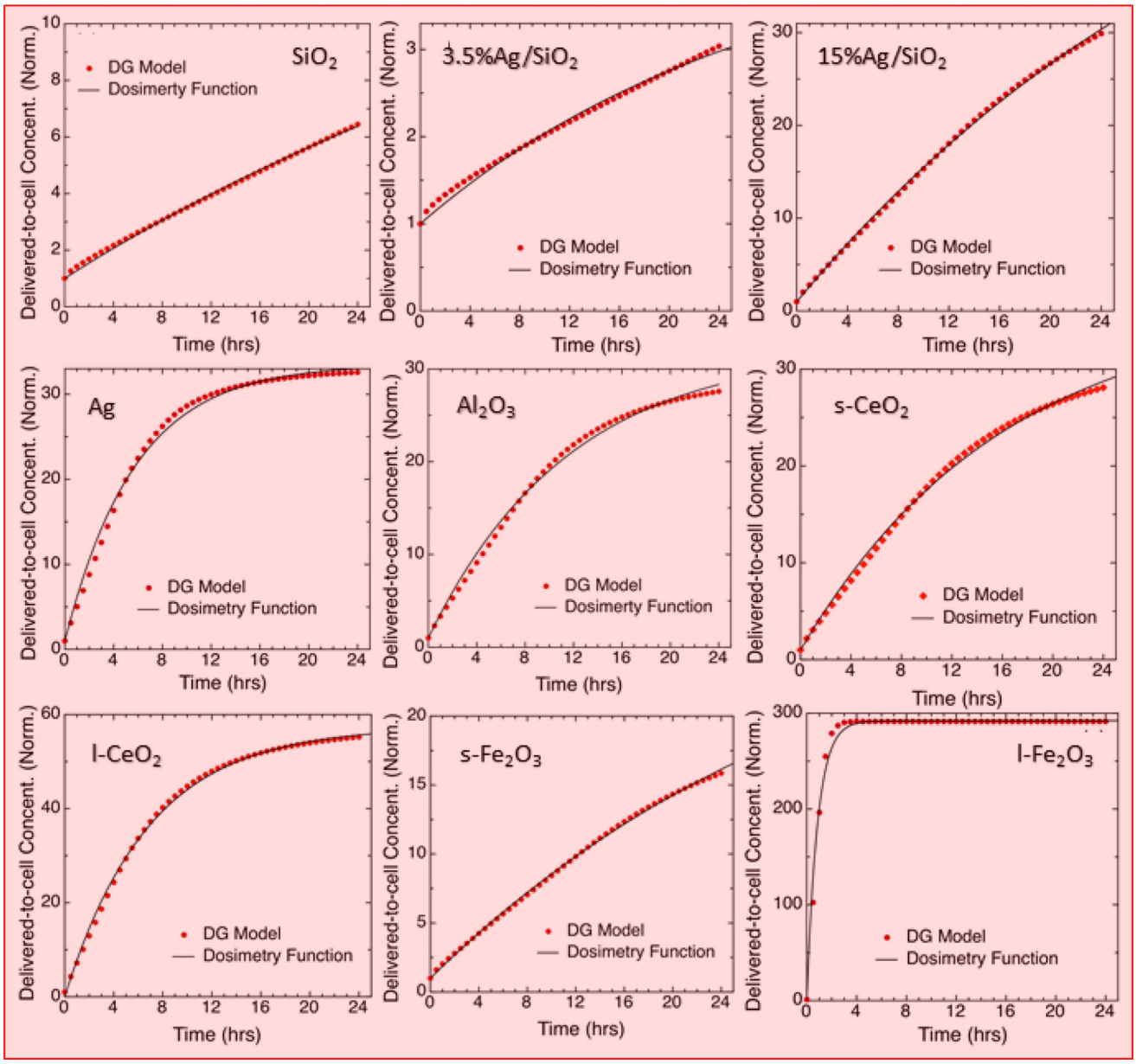

Fig. 3.

Fate and transport modeling results. Delivered-to-cell concentration of nine ENMs normalized to the administered dose. Solid lines are the fitting curves obtained using eq. 2.

Table 1

Morphological and structural properties of ENMs

ENM	Primary Particle Size				Crystal Structure	
	SSA (m^2/g)	d_{BET} (nm)	d_{TEM} (nm)	d_{XRD} (nm)	Crystal System	Crystallinity (%)
SiO_2	152.3±7.5	15.4±1.0	N/A	N/A	N/A	amorphous
Al_2O_3	51.1±1.0	32.6±1.7	28.1±13.1	12.2	monoclinic (52%) orthorhombic (48%)	68
Ag	31.2±0.5	18.3±0.3	25.6±6.5	12.3	cubic	65
3.5%Ag/SiO_2	359.8±14.4	9.3 (Ag) 7.1±0.4 (SiO_2)	10.6±7.1 (Ag)	7.9 (Ag)	cubic	91
15%Ag/SiO_2	333.1±3.1	6.4 (Ag) 6.1±0.1 (SiO_2)	7.9±4.3 (Ag)	5.8 (Ag)	cubic	87
s-CeO_2	129.5±5.2	5.3±0.2	10.5±5.0	7.8	cubic	72
l-CeO_2	28.5±1.1	27.9±1.1	34.7±22.9	36.3	cubic	86
s-Fe_2O_3	130.6±5.2	10.2±0.5	9.9±3.8	6.9	cubic	35
l-Fe_2O_3	11.0±0.4	112.6±4.5	108.9±47.5	46.8	cubic	87

ENM, engineered nanomaterial; SSA by nitrogen adsorption/Brunauer-Emmett-Teller (BET) method; d_{BET}, d_{TEM} and d_{XRD}, particle diameter determined from SSA, transmission electron microscopy (TEM) analysis and X-ray diffraction (XRD), respectively.

Table 2

Physical properties of ENMs

ENM	Shape Factors			Porosity		ρ_{raw} (g/cc)
	Aspect ratio	Circularity	Roundness	TPV (cc/g)	APS[§] (nm)	
SiO_2	N/A	N/A	N/A	0.16	2.2	2.59±0.10
Al_2O_3	1.10±0.11	0.94±0.07	0.92±0.07	0.06	2.3	3.59±0.04
Ag	1.18±0.17	0.92±0.14	0.85±0.10	0.05	3.6	8.34±0.40
3.5%Ag/SiO_2	1.18±0.17	0.92±0.14	0.86±0.11	0.75	4.2	3.24±0.14
15%Ag/SiO_2	1.12±0.14	0.97±0.09	0.89±0.11	0.46	3.7	3.58±0.25
s-CeO_2	1.18±0.17	0.75±0.09	0.74±0.13	1.00	1.9	7.95±0.20
l-CeO_2	1.18±0.17	0.82±0.06	0.77±0.13	0.24	1.7	7.53±0.02
s-Fe_2O_3	1.21±0.20	0.88±0.05	0.84±0.11	0.36	4.5	4.48±0.15
l-Fe_2O_3	1.10±0.07	0.90±0.06	0.91±0.05	0.01	2.9	4.74±0.01

ENM, engineered nanomaterial; TPV and APS, total pore volume and average pore size, respectively determined by nitrogen adsorption/Brunauer-Emmett-Teller (BET) method; ρ_{raw}, the raw density of ENMs determined by nitrogen volume displacement (pycnometry);

[§]TEM did not confirm the presence of pores but interparticle spacing instead.

Table 3

Chemical and biological properties of ENMs

ENM	Chemical Elemental Composition				Recombinant Factor C (EU/mg)[£]	Sterility (bacterial growth observed)[†]
	Trace Metal Analysis (%)	Carbon Content (%)[*]	Stoichiometry XPS	Stoichiometry ICP-MS		
SiO_2	99.98±0.93 Si	0.29±0.13	$SiO_{2.1}$	$SiO_{2.5}$	< LOD	No growth
Al_2O_3	99.97±0.99 Al	0.29±0.19	$Al_2O_{2.9}$	$Al_2O_{3.1}$	< LOD	No growth
Ag	99.01±0.05 Ag	0.20±0.28	N/A	N/A	1.79	No growth
3.5%Ag/SiO_2	99.98±0.03 Ag[≠]	0.05±0.20	$SiO_{2.0}$	N/A	2.65	No growth
15%Ag/SiO_2	99.98±0.03 Ag[§]	0.05±0.17	$SiO_{2.1}$	N/A	23.93	No growth
s-CeO_2	99.90±0.90 Ce	0.54±0.09	$CeO_{2.0}$	$CeO_{2.7}$	<LOD	No growth
l-CeO_2	99.92±0.30 Ce	0.00±0.15	$CeO_{1.9}$	$CeO_{2.3}$	<LOD	No growth
s-Fe_2O_3	99.90±0.30 Fe	0.16±0.22	$Fe_2O_{2.7}$	$Fe_2O_{3.4}$	5.04	No growth
l-Fe_2O_3	99.98±0.10 Fe	0.17±0.21	$Fe_2O_{3.5}$	$Fe_2O_{3.2}$	0.65	No growth

ENM, engineered nanomaterial; LOD, limit of detection;

[*] Elemental plus organic carbon content (w/w);

[£] Suspension tested at 10 μg/ml, endotoxins in PBS is 76 EU/ml;

[†] suspension tested at 50μg/ml;

[≠] Silver content (w/w) 3.79±0.08;

[§] Silver content (w/w) 15.92±0.25.